JOC Article

Bis(*n*-octylamino)perylene-3,4:9,10-bis(dicarboximide)s and Their Radical Cations: Synthesis, Electrochemistry, and ENDOR Spectroscopy

Michael J. Ahrens, Michael J. Tauber, and Michael R. Wasielewski*

Department of Chemistry and Center for Nanofabrication and Molecular Self-Assembly, Northwestern University, Evanston, Illinois 60208-3113

m-wasielewski@northwestern.edu

Received November 20, 2005

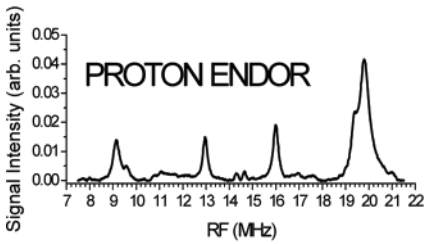

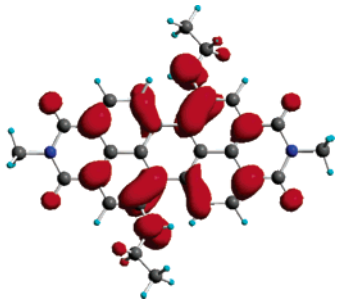

1,6- and 1,7-bis(*n*-octylamino)perylene-3,4:9,10-bis(dicarboximide) were synthesized by reaction of *n*-octylamine with the corresponding dibromo compounds. These compounds display intense charge-transfer optical transitions in the visible spectrum (~550−750 nm) and fluoresce weakly (Φ_F < 0.06). Cyclic voltammetry reveals that each chromophore undergoes facile and reversible oxidation and reduction. Spectroelectrochemical studies show that the radical cations of these chromophores are stable and show no signs of deprotonation of the secondary amines. Electron paramagnetic resonance (EPR) and electron−nuclear double resonance (ENDOR) studies of the chemically generated radical cations of these chromophores corroborate the spectroelectrochemical data by showing that the radical cations persist for days at room temperature in methylene chloride solution. These experiments and complementary density functional theory (DFT) calculations provide a comprehensive picture of the molecular orbitals, spin density distributions, and geometries of the radical cations. The redox properties and stability of these alkylamino-functionalized perylene compounds make them a valuable addition to the family of robust perylene-based chromophores that can be used to develop new photoactive charge transport materials.

Introduction

Perylene-3,4:9,10-bis(dicarboximide) (PDI) and related arylene dicarboximides and bis(dicarboximides) continue to receive considerable attention for applications such as field effect transistors,[1,2] molecular electronics,[3−5] light-harvesting arrays,[6,7] solar cells,[8,9] and light-emitting diodes.[10,11] These chromophores have generated great interest because of their high photochemical stability, ease of synthetic modification, and desirable optical/redox characteristics. The special emphasis on stable, red to

(1) Jones, B. A.; Ahrens, M. J.; Yoon, M.-H.; Facchetti, A.; Marks, T. J.; Wasielewski, M. R. *Angew. Chem., Int. Ed.* **2004**, *43*, 6363−6366.
(2) Chen, Z.; Debije, M. G.; Debaerdemaeker, T.; Osswald, P.; Würthner, F. *ChemPhysChem* **2004**, *5*, 137−140.
(3) Hayes, R. T.; Wasielewski, M. R.; Gosztola, D. *J. Am. Chem. Soc.* **2000**, *122*, 5563−5567.
(4) Davis, W. B.; Svec, W. A.; Ratner, M. A.; Wasielewski, M. R. *Nature* **1998**, *396*, 60−63.
(5) Lukas, A. S.; Bushard, P. J.; Wasielewski, M. R. *J. Am. Chem. Soc.* **2001**, *123*, 2440−2441.
(6) Loewe, R. S.; Tomizaki, K.; Youngblood, W. J.; Bo, Z.; Lindsey, J. S. *J. Mater. Chem.* **2002**, *12*, 3438−3451.
(7) Tomizaki, K.; Loewe, R. S.; Kirmaier, C.; Schwartz, J. K.; Retsek, J. L.; Bocian, D. F.; Holten, D.; Lindsey, J. S. *J. Org. Chem.* **2002**, *67*, 6519−6534.
(8) Gregg, B. A.; Cormier, R. A. *J. Am. Chem. Soc.* **2001**, *123*, 7959−7960.
(9) Breeze, A. J.; Salomon, A.; Ginley, D. S.; Gregg, B. A.; Tillmann, H.; Horhold, H. H. *Appl. Phys. Lett.* **2002**, *81*, 3085−3087.
(10) Angadi, M. A.; Gosztola, D.; Wasielewski, M. R. *Mater. Sci. Eng. B* **1999**, *63*, 191−194.
(11) Ranke, P.; Bleyl, I.; Simmerer, J.; Haarer, D.; Bacher, A.; Schmidt, H. W. *Appl. Phys. Lett.* **1997**, *71*, 1332−1334.

10.1021/jo052394o CCC: $33.50
Published on Web 02/09/2006

near-infrared (NIR) absorbing chromophores is driven by the demands of optoelectronic and solar cell applications. For example, chromophores with lengthened conjugated cores (extended transition dipoles), such as derivatives of terrylene and quaterrylene bis(dicarboximides), have excellent red and NIR absorption characteristics.[12−14]

The electronic characteristics of arylene imides and diimides can be tuned to some degree using the imide functionality,[15] but the nodes in both the HOMO and LUMO that bisect these molecules through their long axes limit electronic coupling through this linkage. The most effective method of changing the electronic absorption characteristics of these molecules is direct substitution of the conjugated aromatic core. Substitution of the core with electron-donating groups has yielded alkylamino-substituted naphthalene-1,8:4,5-bis(dicarboximide)s,[16] pyrrolidinyl-substituted perylene-3,4:9,10-bis(dicarboximide)s,[17,18] 9-aminoperylene-3,4-dicarboximides,[19] piperidinyl-substituted perylene-3,4:9.10-bis(dicarboximide)s,[20] and terrylene-3,4:11,12-bis(dicarboximide)s.[12] The amino-substituted arylene bis(dicarboximide)s display strongly red-shifted absorption and emission bands and are oxidized and reduced with ease. By contrast, most other arylene bis(dicarboximide)s are generally difficult to oxidize due to stabilization of the HOMO by the electron-withdrawing imide groups. Most examples in the literature report enhancement of their good electron-accepting properties, the most extreme example being the cyanated derivatives.[21]

This paper focuses on derivatives of perylene-3,4:9,10-bis(dicarboximide), PDI. To date, there are two principal methods for introducing substituents onto the PDI core. The first method is 4-fold symmetric chlorination of the 1, 6, 7, and 12 positions,[22,23] while the second method is bromination of perylene dianhydride,[18,24] which yields the desired 1,7-dibrominated product but also produces a varying amount of the difficult to separate 1,6-dibrominated side product. Replacement of these halogens is readily achieved by traditional substitution reactions or metal-catalyzed cross-coupling reactions,[25−27] although the former are sometimes accompanied by extensive debromination. In an effort to expand the scope of chromophores available for designing systems for self-assembly and charge transport based on PDI, we have investigated substitution of bay region bromines by *flexible* alkylamino substituents, since previous studies from our laboratory and others[17,18,20,28−38] have used only sterically bulky cyclic amines as electron-donating groups. We now report on the introduction of *n*-octylamino groups at the 1,6- and 1,7-positions of PDI affording chromophores that are either intense blue **(1,6)** or green **(1,7)** in color and that readily undergo both one-electron oxidations and reductions. In particular, the radical cations **(1,6)**$^{\bullet+}$ and **(1,7)**$^{\bullet+}$ are unusually stable.

Results and Discussion

Synthesis. The synthetic scheme for **(1,6)** and **(1,7)** is given in Figure 1. Bromination of PDI leads to a mixture of isomers in which the 1,7 isomer usually dominates.[18,20] The isomeric mixture *N*,*N*′-bis(*n*-octyl)(1,6- and 1,7-dibromoperylene-3,4:9,10-bis(dicarboximide) was heated in neat *n*-octylamine to obtain the corresponding secondary amines **(1,6)** and **(1,7)** as well as the 1-(*n*-octylamino) derivative as a consequence of partial debromination of the starting material. The 1-(*n*-octylamino) derivative was separated from **(1,6)** and **(1,7)** by column chromatography, while **(1,6)** and **(1,7)** were separated from each other by preparative HPLC.

Photophysical Characterization. The ground-state absorption spectra of the green **1,7** isomer and the blue **1,6** isomer in toluene are shown in Figure 2. The spectra are dominated by very broad, and nearly structureless, absorption bands that span a large part of the visible spectrum (475−750 nm for **1,6** and 550−750 nm for **1,7**). This broad absorption is strongly red-shifted relative to that of unsubstituted PDI, is very similar to spectra of PDIs substituted at the 1,7 positions with secondary cyclic amine substituents, and is characteristic of charge transfer (CT) excited states.[17] The main differences between the two spectra are the absorption near 400 nm for the **1,7** isomer and the peak at ∼545 nm in the spectrum of the **1,6** isomer. These two features account for the large difference in color observed by the naked eye.

Both isomers are soluble in a wide range of solvents including hexane, methylcyclohexane, toluene, chloroform, dichloromethane, and butyronitrile. In previous work, preferential solvation of long, aliphatic tails served to assemble various PDI

(12) Nolde, F.; Qu, J.; Kohl, C.; Pschirer, N. G.; Reuther, E.; Müllen, K. *Chem. Eur. J.* **2005**, *11*, 3959−3967.
(13) Langhals, H.; Büttner, J.; Blanke, P. *Synthesis* **2005**, *3*, 364−366.
(14) Geerts, Y.; Quante, H.; Platz, H.; Mahrt, M.; Hopmeier, M.; Böhm, A.; Müllen, K. *J. Mater. Chem.* **1998**, *8*, 2357−2369.
(15) Quante, H.; Geerts, Y.; Müllen, K. *Chem. Mater.* **1997**, *9*, 496−500.
(16) Thalacker, C.; Miura, A.; De Feyter, S.; DeSchryver, F. C.; Würthner, F. *Org. Biomol. Chem.* **2005**, *3*, 414−422.
(17) Zhao, Y.; Wasielewski, M. R. *Tetrahedron Lett.* **1999**, *40*, 7047−7050.
(18) Würthner, F.; Stepanenko, V.; Chen, Z.; Saha-Moeller, C. R.; Kocher, N.; Stalke, D. *J. Org. Chem.* **2004**, *69*, 7933−7939.
(19) Becker, S.; Böhm, A.; Müllen, K. *Chem. Eur. J.* **2000**, *6*, 3984−3989.
(20) Rohr, U.; Kohl, C.; Müllen, K.; van de Craats, A.; Warman, J. *J. Mater. Chem.* **2001**, *11*, 1789−1799.
(21) Ahrens, M. J.; Fuller, M. J.; Wasielewski, M. R. *Chem. Mater.* **2003**, *14*, 2684−2686.
(22) Iden, R.; Seybold, G. (BASF AG: Germany) *Chem. Abstr.* **1985**, *103*, 38696q.
(23) Sandrai, M.; Hadel, L.; Sauers, R. R.; Husain, S.; Krogh-Jespersen, K.; Westbrook, J. D.; Bird, G. R. *J. Phys. Chem.* **1992**, *96*, 7988−7996.
(24) Böhm, A.; Arms, H.; Henning, G.; Blaschka, P. BASF German Patent No. DE 19547209A1, 1997.
(25) Ahrens, M. J.; Sinks, L. E.; Rybtchinski, B.; Liu, W.; Jones, B. A.; Giaimo, J. M.; Gusev, A. V.; Goshe, A. J.; Tiede, D. M.; Wasielewski, M. R. *J. Am. Chem. Soc.* **2004**, *126*, 8284−8294.
(26) Ego, C.; Marsitzky, D.; Becker, S.; Zhang, J.; Grimsdale, A. C.; Müllen, K.; MacKenzie, J. D.; Silva, C.; Friend, R. H. *J. Am. Chem. Soc.* **2003**, *125*, 437−443.
(27) Chen, S.; Liu, Y.; Qiu, W.; Sun, X.; Ma, Y.; Zhu, D. *Chem. Mater.* **2005**, *17*, 2208−2215.
(28) Fuller, M. J.; Walsh, C. J.; Zhao, Y.; Wasielewski, M. R. *Chem. Mater.* **2002**, *14*, 952−953.
(29) Giaimo, J. M.; Gusev, A. V.; Wasielewski, M. R. *J. Am. Chem. Soc.* **2002**, *124*, 8530−8531.
(30) Lukas, A. S.; Zhao, Y.; Miller, S. E.; Wasielewski, M. R. *J. Phys. Chem. B.* **2002**, *106*, 1299−1306.
(31) Rybtchinski, B.; Sinks, L. E.; Wasielewski, M. R. *J. Am. Chem. Soc.* **2004**, *126*, 12268−12269.
(32) Fuller, M. J.; Sinks, L. E.; Rybtchinski, B.; Giaimo, J. M.; Li, X.; Wasielewski, M. R. *J. Phys. Chem. A.* **2005**, *109*, 970−975.
(33) Fan, L.; Xu, Y.; Tian, H. *Tetrahedron Lett.* **2005**, *46*, 4443−4447.
(34) Yukruk, F.; Dogan, A. L.; Canpinar, H.; Guc, D.; Akkaya, E. U. *Org. Lett.* **2005**, *7*, 2885−2887.
(35) Franceschin, M.; Alvino, A.; Ortaggi, G.; Bianco, A. *Tetrahedron Lett.* **2004**, *45*, 9015−9020.
(36) Sugiyasu, K.; Fujita, N.; Shinkai, S. *Angew. Chem., Int. Ed.* **2004**, *43*, 1229−1233.
(37) Langhals, H.; Blanke, P. *Dyes Pigments* **2003**, *59*, 109−116.
(38) Serin, J. M.; Brousmiche, D. W.; Frechet, J. M. J. *J. Am. Chem. Soc.* **2002**, *124*, 11848−11849.

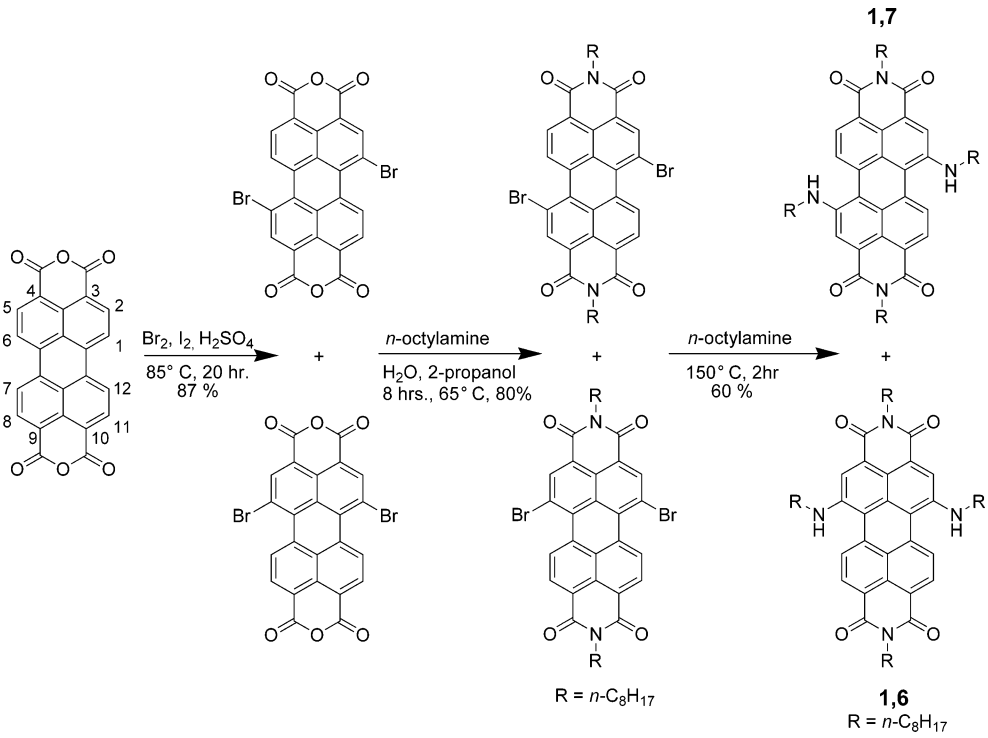

FIGURE 1. Synthetic scheme.

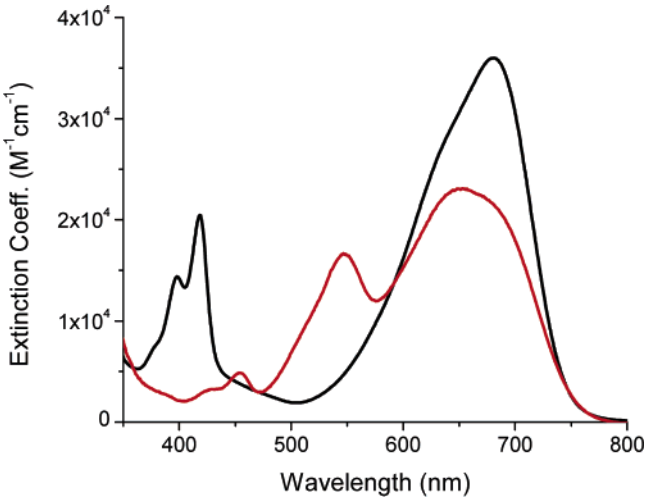

FIGURE 2. Ground-state absorption spectra for **(1,7)** (black) and **(1,6)** (red) in toluene.

chromophores into either *H*-[32] or *J*-type[39,40] aggregates. However, in this study, only the monomeric spectrum is observed in all solvents investigated, indicating little or no aggregation up to concentrations of ~1 mM. The only observable difference between solvents is a red shift in the absorbance spectrum upon increasing solvent polarity: **1,7**, λ_{max}= 658 nm in hexane and 705 nm in DMF; **1,6**, λ_{max}= 624 nm in hexane and 675 nm in DMF. We attribute the shift to increased stabilization of the CT excited state.

Using the well-established fluorescence solvatochromic shift method,[41] we measured the stabilization of the excited-states of **1,6** and **1,7** and compared these results to those for 1,7-bis(pyrrolidin-1-yl)perylene-3,4:9,10-bis(dicarboximide) (**5PDI**)[30] and the monosubstituted *N*,*N*′-bis(*n*-octyl)-1-(*n*-octylamino)-perylene-3,4:9,10-bis(dicarboximide). The emission λ_{max} of each compound was measured in eight solvents with dielectric constants ranging from 2.02 to 36.7 and plotted against $f(\epsilon,n) = [(\epsilon - 1)/(2\epsilon + 1) - 0.5\ (n^2 - 1)/(2n^2 + 1)]$, where ϵ and n are the static dielectric constant and the refractive index of the solvent, respectively, to give the Lippert−Mataga plots shown in Figure 3. The change in dipole moment from ground to excited-state $\Delta\mu_{ge}$ determined from this plot is highly dependent on the Onsager radius;[41] therefore, we report a range of $\Delta\mu_{ge}$ values that result from radii spanning 5.0−7.5 Å, with the upper limit obtained from AM1 optimization using Gaussian 98. For the **1,7** isomer, $\Delta\mu_{ge}$ = 7.7−14.2 D, while for the **1,6** isomer, $\Delta\mu_{ge}$ = 10.0−18.4 D. These values of $\Delta\mu_{ge}$ are very close to those determined for **5PDI** (7.4−13.6 D) and monosubstituted *N*,*N*′-bis(*n*-octyl)-1-(*n*-octylamino)perylene-3,4:9,10-bis(dicarboximide) (7.7−14.2 D).

The ground-state dipole moments obtained by DFT calculations at the B3LYP/6-31G* level are 0.0 D for the centrosymmetric **1,7** isomer, and 1.0 D for the asymmetric **1,6** isomer. Therefore the $\Delta\mu_{ge}$ values obtained above reflect the formation of a substantial dipole moment in the equilibrium excited state. The most likely molecular origin of this dipole is charge transfer from one amino substituent to the perylene core. This asymmetric CT process readily explains why the centrosymmetric **1,7** isomer has an overall excited state dipole moment. The hypothesis is also consistent with the nearly identical excited state stabilization measured experimentally for the monosubstituted alkylamino-PDI and the **1,7** isomer. The formation of substantial excited-state dipole moments in other symmetric molecules in solution, due to asymmetric or local excitation,

(39) van Herrikhuyzen, J.; Syamakumari, A.; Schenning, A. P. H. J.; Meijer, E. W. *J. Am. Chem. Soc.* **2004**, *126*, 10021−10027.

(40) Würthner, F.; Thalacker, C.; Diele, S.; Tschierske, C. *Chem.*−*Eur. J.* **2001**, *7*, 2245−2253.

(41) Lakowicz, J. R. *Principles of Fluorescence Spectroscopy*, 2nd ed.; Kluwer Academic/Plenum Publishers: New York, 1999.

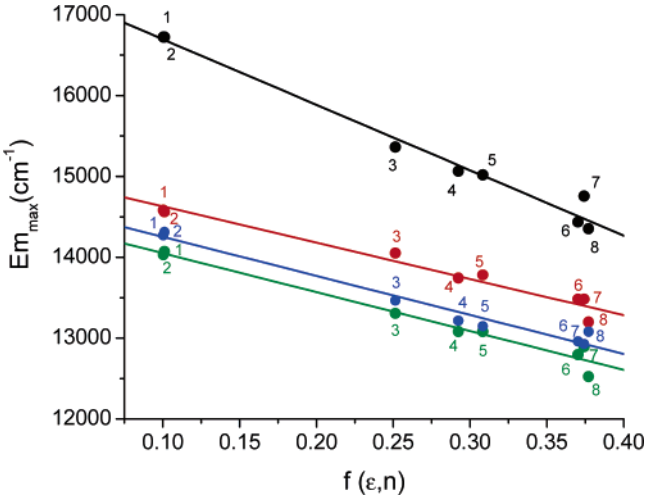

FIGURE 3. Lippert−Mataga plots for **(1,7)** (green dots, $R^2 = 0.984$), **(1,6)** (black dots, $R^2 = 0.991$), **5PDI** (red dots, $R^2 = 0.947$), *N*,*N*′-bis-(*n*-octyl)-1-(*n*-octylamino)perylene-3,4:9,10-bis(dicarboximide) (blue dots, $R^2 = 0.975$). The solvents are (1) methylcyclohexane, (2) cyclohexane, (3) ethyl ether, (4) ethyl acetate, (5) tetrahydrofuran, (6) butyronitrile, (7) acetone, and (8) DMF.

have been reported previously.[42,43] An alternative explanation for the excited-state stabilization, in which the symmetry of the ground state is maintained, is local solvation differences between the two equivalent aminoperylene dipoles oriented in opposition along the short axis of perylene. The net stabilization in this scenario is best described in terms of quadrupole-solvent dipole interactions.[44] Although we cannot rule out this explanation, it is less likely since it requires a fortuitous coincidence in the overall stabilization of the monosubstituted and **1,7** symmetrically disubstituted molecules.

The ground-state geometries determined by DFT(B3LYP/6-31G*) calculations have a core twist angle of the perylene core, i.e., the approximate dihedral angle between the two naphthalene subunits attached to the central benzene ring, which is 14.9° for the **1,7** isomer and 21.7° for the **1,6** isomer, Figure 4. For comparison, the 1,7-dibrominated PDI derivative has a measured core twist angle of 24°.[2] There are very few literature examples of 1,6-disubstituted PDIs and to our knowledge no measured crystal structures. As a whole, the alkylamino PDI chromophores have smaller calculated core twist angles than those obtained from X-ray crystal structures of other PDI derivatives.[2] The experimental 620 cm^{-1} difference in energy at λ_{max} between the **1,6** and **1,7** isomers in hexane, Table 1, agrees reasonably well with the calculated difference in HOMO−LUMO gaps between the two isomers (985 cm^{-1}, Table 2). As expected, the calculation for the flatter **1,7** isomer yields a HOMO−LUMO gap which is smaller than that of the more twisted **1,6** isomer.

Electrochemistry and Spectroelectrochemistry. The redox potentials of the **1,6** and **1,7** isomers (Table 3) are obtained by cyclic voltammetry. Both isomers show two oxidation and two reduction waves. All are chemically reversible, with 60−90 mV peak separations, except for the second oxidation of the **1,6**-isomer. Differential pulse voltammetry (DPV) was used to determine the potential of the second irreversible oxidation process for **(1,6)** at +1.06 V. The intensity of this peak was lower than that of the first oxidation peak, most likely due to irreversible decomposition of the dication. We note that the first oxidation potential of **(1,6)** (+0.91 V) is considerably more positive than that of **(1,7)** (+0.76 V), and that the reduction potentials are identical within experimental error. The energies of the LUMOs and HOMOs determined by the DFT calculations (Table 2) closely reflect the experimental trends: the HOMO of the **1,6** isomer is 0.11 eV lower in energy than that of the **1,7** isomer, and the LUMO energy of the **1,6** isomer is 0.01 eV lower than that of **1,7**; both of these calculated values correspond well to the respective 0.15 and 0.01 V experimental differences.

Spectroelectrochemical oxidation of **1,7** shows the growth of prominent new absorption features at 918 and 1068 nm, which are attributed to the radical cation **(1,7)**$^{\bullet+}$, Figure 5A. Full reversibility over as much as 40 min attests to the stability of the radical cation. Nearly identical spectra of **(1,7)**$^{\bullet+}$ are obtained upon chemical oxidation with $NOSbF_6$ (Figure S1). The stability of the chemically oxidized samples is remarkable: the cation bands show only 50% diminishment after 6 days of storage at room temperature in a sealed tube. The NIR bands resemble those previously observed for the cyclic amino-substituted perylenes substituted at the 1,7 positions.[30] The DFT results help rationalize the appearance of the new features in the NIR, since the calculated gap between (HOMO-1) and HOMO of **(1,7)** is 8884 cm^{-1}, close to the energy of the experimentally observed transitions.

In the case of **(1,6)**, spectroelectrochemical oxidation yields a spectrum that differs only slightly from the neutral parent, with the main change being the growth of a new band with a maximum at 616 nm (Figure 5B). A chemically oxidized sample shows similar spectral changes (Figure S1, Supporting Information) and exhibits EPR and ENDOR signals (described below); thus, we assign the new spectrum to the radical cation. The prominent NIR absorption bands that are typical of the radical cations of **1,7**-substituted alkyl-amino PDIs are absent from all spectra obtained after electrochemical or chemical oxidation of the **1,6** isomer, including samples that are oxidized further than those shown in Figure 5B (not shown). The DFT results support the assignment of the new spectrum with a maximum at 616 nm to the radical cation. The calculated (HOMO-1)−HOMO energy gap for **(1,6)** is only 5048 cm^{-1}, which is consistent with the lack of absorption features in the 800−1100 nm region for **(1,6)**$^{\bullet+}$.

Our observation of stable and reversible electrochemical/chemical production of long-lived **(1,6)**$^{+\bullet}$ and **(1,7)**$^{+\bullet}$ species is noteworthy. Generally, electrochemical oxidation of aliphatic amines is irreversible because formation of the amine radical cation leads to dealkylation, proton loss, or nucleophilic attack.[45−50] Substitution of the amine with aromatic groups stabilizes the radical cation, as has been demonstrated in some aniline derivatives.[51] Maroz et al.[52] have shown that geometry

(42) Bangal, P. R.; Lam, D. M. K.; Peteanu, L. A.; Van der Auweraer, M. *J. Phys. Chem. B* **2004**, *108*, 16834−16840.
(43) Piet, J. J.; Schuddeboom, W.; Wegewijs, B. R.; Grozema, F. C.; Warman, J. M. *J. Am. Chem. Soc.* **2001**, *123*, 5337−5347.
(44) Ghoneim, N.; Suppan, P. *Spectrochim. Acta, Part A* **1995**, *51*, 1043−1050.
(45) Portis, L. C.; Bhat, V. V.; Mann, C. K. *J. Org. Chem.* **1970**, *35*, 2175−2178.
(46) Smith, P. J.; Mann, C. K. *J. Org. Chem.* **1969**, *34*, 1821−1826.
(47) Mann, C. K. *Anal. Chem.* **1964**, *36*, 2424−2426.
(48) Masui, M.; Sayo, H. *J. Chem. Soc. B: Phys. Org.* **1971**, *8*, 1593−1596.
(49) Barnes, K. K.; Mann, C. K. *J. Org. Chem.* **1967**, *32*, 1474−1479.
(50) Dapo, R.; Mann, C. K. *Anal. Chem.* **1963**, *35*, 677−680.
(51) Saito, F.; Tobita, S.; Shizuka, H. *J. Photochem. Photobiol., A: Chem.* **1997**, *106*, 119−126.

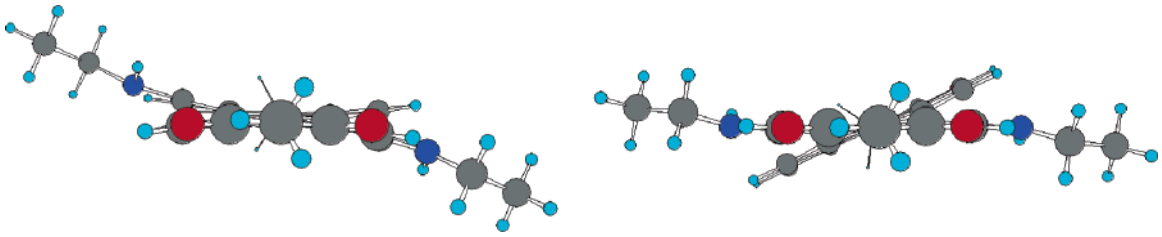

FIGURE 4. DFT (B3LYP/6-31G*) geometry-optimized structures of **(1,7)** (left) and **(1,6)** (right) shown with view along the long axis. For the purposes of the computation, ethyl groups replace the *n*-octyl amino groups and methyls replace the octyls at the imide positions. The "core-twist angle" for **(1,7)** is 14.9° and for **(1,6)** is 21.7°.

TABLE 1. Absorption and Emission Maxima and Fluorescence Quantum Yields (Φ_F)

	λ_{abs} (nm)				λ_{em} (nm)		Φ_F[c]	
	toluene	THF	CH_2Cl_2	hexane	toluene	THF	toluene	THF
(**1,6**)	653.5	660	657	634	772[a]	793[a]	<0.01	<0.01
(**1,7**)	681	682	692	656.5	743[b]	766[b]	0.06	0.02

[a] 580 nm excitation. [b] 550 nm excitation. [c] Oxazine 170 relative standard (0.63 in methanol).

TABLE 2. Molecular Orbital Energies from DFT Calculations

	(1,6) (eV)		**(1,7)** (eV)	
LUMO (eV)	−2.9973		−3.0069	
HOMO (eV)	−5.2556		−5.1430	
HOMO-1 (eV)	−5.8815		−6.2445	
energy gap (cm^{-1})	18213[a]	5048[b]	17228[a]	8884[b]

[a] HOMO−LUMO. [b] HOMO−(HOMO-1).

TABLE 3. Oxidation and Reduction Potentials vs SCE[a]

compd	$E^{-}_{1/2}$	$E^{2-}_{1/2}$	$E^{+}_{1/2}$	$E^{2+}_{1/2}$
(**1,6**)	−0.84	−1.03	0.91	1.06[b]
(**1,7**)	−0.83	−1.00	0.76	0.95

[a] Values obtained by cyclic voltammetry (except as noted) in dry CH_2Cl_2 with 0.1 M Bu_4NPF_6 as the supporting electrolyte and Fc/Fc^+ as internal standard. [b] Value from minor peak of differential pulse voltammogram (not shown).

plays an important role in stabilizing aromatic amines. In the case of *N*-methylaniline, the *planar* geometry (proton in aromatic plane) is not susceptible to deprotonation, whereas the *perpendicular* geometry (proton out of aromatic plane) undergoes loss of a proton at the diffusion-limited rate. In our case, DFT calculations show that the amine protons of **(1,6)** and **(1,7)** are nearly in the plane of the perylene core at their respective points of attachment in both their neutral and oxidized states, which is consistent with the stability to proton loss observed experimentally.

Electron Paramagnetic Resonance. The EPR and ENDOR spectra acquired upon reaction of **(1,6)** or **(1,7)** with $NOSbF_6$ in CH_2Cl_2 at room temperature reinforce the conclusion that these electron-rich PDIs form reasonably stable radical cations. Broadened CW-EPR spectra are obtained at 270 K, with *g* values of 2.0025 for **(1,6)**$^{\bullet+}$ and 2.0027 for **(1,7)**$^{\bullet+}$, Figure 6. Remarkably, the same EPR spectra were acquired on these samples after storage at room temperature for nearly one week, albeit at reduced intensity. The signal of **(1,6)**$^{\bullet+}$ was diminished by about 80%, while that for **(1,7)**$^{\bullet+}$ was reduced by only 50%.

Isotropic hfcc's were obtained from ENDOR spectroscopy in liquid CH_2Cl_2 solution using the ENDOR resonance condition $\nu_{ENDOR} = |\nu_n \pm a/2|$ where ν_{ENDOR} are the ENDOR transition frequencies, ν_n is the proton Larmor frequency, and a is the isotropic hyperfine coupling constant (hfcc).[53] The ENDOR spectrum of **(1,7)**$^{\bullet+}$, Figure 7, shows four distinct peak pairs, of which the three largest are within 25% of hfcc's determined by DFT calculation, Table 4. The calculation leads to assignment of the 3.51 G resonance to the two amine protons, and the 3.81 G resonance to the four methylene protons nearest the amine. The experimental peak at 1.09 G is assigned to the bay region proton. The smallest ENDOR peak at 0.14 G is likely due to one of the two other perylene proton pairs, although definitive assignment is not possible since the calculation suggests that two resonances should be observed at 0.36 and 0.18 G. The simulation of the CW-EPR spectrum of **(1,7)**$^{\bullet+}$ (Winsim)[54] using the ENDOR results to lock the proton assignments, allows assignment of the nitrogen resonances. Only the hyperfine coupling constant of the secondary amine nitrogens is large. The DFT result for the coupling constant is in rough agreement with the value obtained from the simulation. The spin densities at each atomic center show that the unpaired electron is most strongly associated with the secondary amine nitrogens. The greatest spin density on the perylene core of **(1,7)**$^{\bullet+}$ is distributed centrosymmetrically on eight carbons, Figure 8. There are distinct nodes in the spin density, which is fully consistent with the small coupling constants for the imide nitrogens, as well as outer protons 2, 5, 8, and 11 of the perylene core.

The EPR and ENDOR spectra of the **(1,6)**$^{\bullet+}$-isomer are shown in Figures 6 and 7, respectively. Hfcc's determined from these spectra (Table 4) clearly show that the amine groups of **(1,6)**$^{\bullet+}$ have less unpaired spin density than **(1,7)**$^{\bullet+}$, as shown by the smaller coupling constants of amino-alkyl protons and amine nitrogens. On the other hand, there is considerable spin density on the perylene core of **(1,6)**$^{\bullet+}$ which is concentrated on the half of the aromatic system that is farthest from the amine substituents. This results in a ~4-fold increase in the hfcc's of the perylene bay protons of **(1,6)**$^{\bullet+}$, relative to **(1,7)**$^{\bullet+}$. The asymmetric substitution also causes the imide nitrogen farthest from the secondary amines to acquire additional spin density, which is unusual since the imide nitrogens are a well-known location for the position of a node in both the HOMO and LUMO.[55] It is clear from the experimental results, and the spin density maps determined computationally (Figure 8) that the substitution pattern strongly affects the electronic structure of the radical cations of these amine-substituted PDIs.

(52) Maroz, A.; Hermann, R.; Naumov, S.; Brede, O. *J. Phys. Chem. A.* **2005**, *109*, 4590−4596.

(53) Kurreck, H.; Kirste, B.; Lubitz, W. *Electron Nuclear Double Resonance Spectroscopy of Radicals in Solution*; VCH: Weinheim, 1988.

(54) Duling, D. R. *J. Magn. Reson. Ser. B* **1994**, *104*, 105−110.

(55) Würthner, F. *Chem. Commun.* **2004**, *14*, 1564−1579.

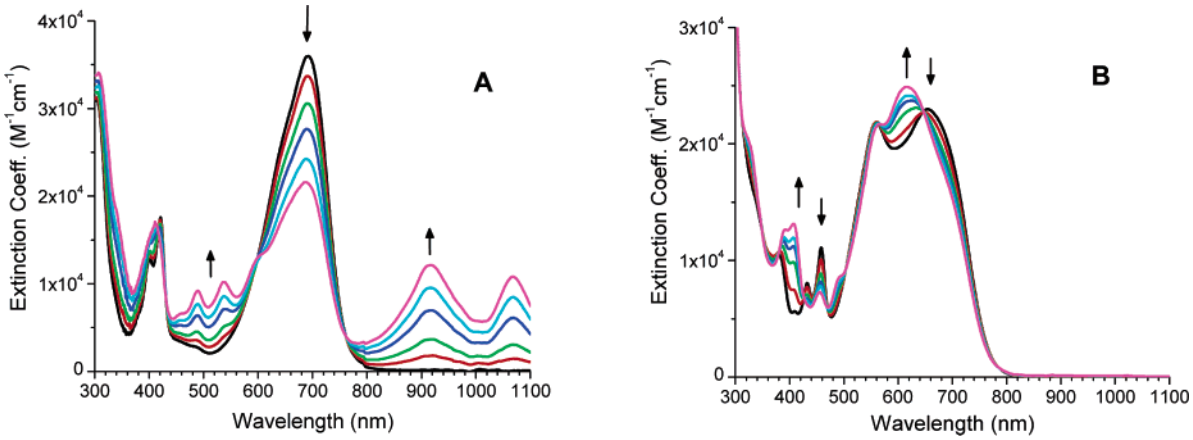

FIGURE 5. Spectroelectrochemistry of (A) **(1,7)** and (B) **(1,6)** in CH_2Cl_2 with 0.1 M Bu_4NPF_6. The purple spectra are those of $\mathbf{(1,7)}^{+\bullet}$ and $\mathbf{(1,6)}^{+\bullet}$ following complete one-electron oxidation of the samples.

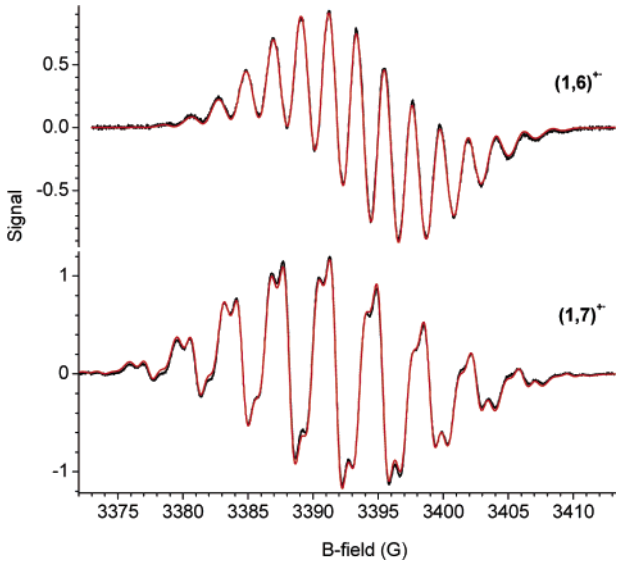

FIGURE 6. CW-EPR spectra (black line) of $\mathbf{(1,6)}^{+\bullet}$ (top) and $\mathbf{(1,7)}^{+\bullet}$ (bottom) in CH_2Cl_2 at 270 K and simulated fits (red line). Sample concentration 0.23 mM of radical cation. Microwave power 6.2 mW, modulation frequency 25 kHz, modulation amplitude 0.25 G. Simulations of the CW spectra are constrained by ENDOR data for protons, and the hfcc's for nitrogen are optimized.

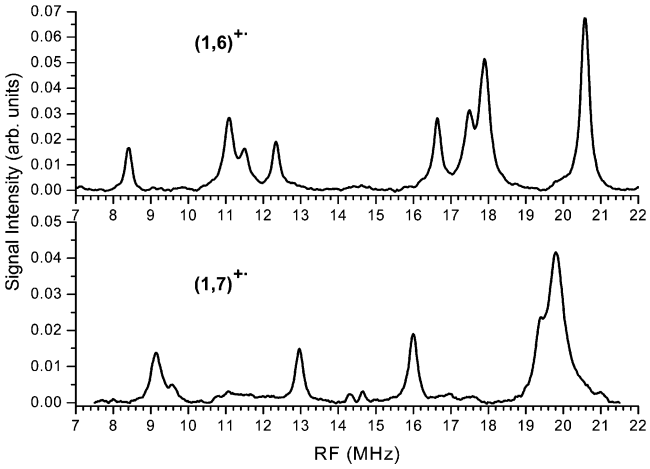

FIGURE 7. ENDOR spectra of 0.23 mM $\mathbf{(1,6)}^{+\bullet}$ and $\mathbf{(1,7)}^{+\bullet}$ in CH_2Cl_2 at 270 K. An off-resonance background is subtracted, and spectra are integrated. $\mathbf{(1,6)}^{+\bullet}$: microwave power 39 mW, RF power 200−600 W across scan range. $\mathbf{(1,7)}^{+\bullet}$: microwave power 99 mW, RF power 300−800 W across scan range. Frequency modulation $\nu_{FM} = 25$ kHz, with modulation depth $\Delta\nu_{RF} = 100$ kHz. 50 scans × 21 s/scan. Note: the conversion factor 2.80 MHz/gauss for comparison with the data presented in Table 4.

Conclusions

The novel chromophores **(1,6)** and **(1,7)** have photophysical and redox properties that will make them useful in the design of new photofunctional electron donor−acceptor systems. Their oxidation and reduction at modest potentials make these chromophores both good electron donors and acceptors. The radical cations exhibit excellent stability at room temperature as shown by cyclic voltammetry, spectroelectrochemistry, and EPR/ENDOR spectroscopy. This stability is noteworthy in view of numerous studies pointing toward oxidative degradation of secondary *N*-alkyl-*N*-arylamines. We hypothesize that the geometry of the secondary amine relative to the aromatic core promotes the observed stability of the radical cations. These compounds offer an additional avenue for expanding the already rich chemistry of PDIs. Further work is underway to expand the applicability of these chromophores to organic electronic materials by functionalizing their imide positions.

Experimental Section

Proton nuclear magnetic resonance spectra were obtained at 500 MHz using TMS as an internal standard. High-resolution mass spectrometry was performed using a spectrometer equipped with a FAB ion source. Laser desorption mass spectra were obtained with a MALDI-TOF mass spectrometer using dithranol as a matrix. Phase transitions were determined using a DSC system.

Synthesis/Purification. *N,N′*-Bis(*n*-octyl)(1,6- and 1,7-*n*-octylamino)perylene-3,4:9,10-bis(dicarboximide). *N,N′*-Bis(*n*-octyl)-(1,6- and 1,7-dibromoperylene-3,4:9,10-bis(dicarboximide)[20] (0.080 g, 0.104 mmol) and *n*-octylamine (3.128 g, 24.2 mmol) were added to a flame-dried 25 mL round-bottom flask. The contents were heated at 150 °C for 2 h under a nitrogen atmosphere. The color of the solution quickly turned from red to green. The hot solution was poured into a solution of methanol/HCl (90/10 mL) and was cooled at 0 °C overnight. The precipitate was collected by centrifugation, washed several times with methanol, and dried with nitrogen to give a green residue. The crude material was purified via flash column chromatography on silica gel using methylene chloride as the eluent to give a mixture of the 1,6 and 1,7 isomers as a green solid, 0.054 g (0.062 mmol), 60%. Additionally, a

TABLE 4. Hyperfine Coupling Constants (Gauss) for $(1,7)^{+\bullet}$ and $(1,6)^{+\bullet}$ As Determined by Proton cw-ENDOR, Simulation of the cw-EPR Spectrum, and DFT Electronic Structure Calculations of Model Compounds Described in the Text

		H	H	H	H		N	N	N
ENDOR	$(1,7)^+$	3.81	3.5	1.09	0.14				
	$(1,6)^+$	2.43	2.14	4.34	1.53				
CW-EPR simulation[1]	$(1,7)^+$	3.81 × 4	3.5 × 2	1.09 × 2	0.14 × 2		3.46 × 2	0.12 x2	
	$(1,6)^+$	2.43 × 4	2.14 × 2	4.34 × 2	1.53 × 2		1.94 × 2		0.54 x1
DFT Calculation	$(1,7)^+$	+3.94	−3.26	−1.36	+0.36	+0.18	+2.69	−0.23	
	$(1,6)^+$	+2.56	−2.1	−4.72	+0.15	+2.11	+1.76	−0.10	−0.45
assignment[2]	$(1,7)^+$	CH_2	N−H	6,12	2,8	5,11	N−H	3,4	9,10
	$(1,6)^+$	CH_2	N−H	7,12	2,5	8,11	N−H	3,4	9,10

[a] Proton hfcc's are from the ENDOR spectra; nitrogen hfcc's are optimized in the simulation.

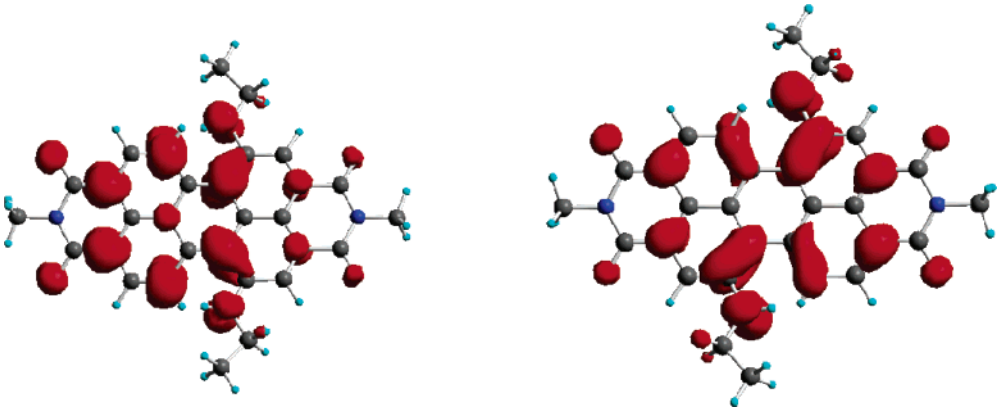

FIGURE 8. Total spin density of model compounds for **(1,6)**$^{+\bullet}$ (left) and **(1,7)**$^{+\bullet}$ (right). The geometries of the radical cations are fully optimized at the unrestricted B3LYP/6-31G* level. The value of $\langle S^2 \rangle = 0.75$ for each calculated radical cation.

significant amount of monosubstituted product *N,N′*-bis(*n*-octyl)-1-(*n*-octylamino)perylene-3,4:9,10-bis(dicarboximide) was isolated and characterized (0.018 g, 0.024 mmol, 23.4%).

Separation of the 1,6 and 1,7 isomers was performed on a preparative HPLC system equipped with a dual-wavelength absorbance detector and fitted with a macro-HPLC column (Si, 8 μm, 250 × 22 mm). The eluent was 3:1 hexanes/chloroform flowing at 12 mL/min. Typical injection volumes were 200 μL of a saturated solution (hexanes) that had been passed through a 0.45 μm PTFE filter prior to injection. Three fractions were collected from the column; the first was pure 1,7 isomer, the second was a mixture of 1,7 and 1,6 isomers, and the third was pure 1,6 isomer. On the basis of analytical HPLC analysis the ratio of 1,7:1,6 isomers can vary from 90:10 to 80:20; see Figure S2, Supporting Information. This reflects the isomeric ratio of the dibrominated starting material.

***N,N′*-Bis(*n*-octyl)-1,7-bis(*n*-octylamino)perylene-3,4:9,10-bis(dicarboximide):** ^{1}H NMR ($CDCl_3$, 500 MHz, see Figure S3, Supporting Information) δ 8.733 (d, J = 8.1 Hz, 2H), 8.288 (d, J = 8.1 Hz, 2H), 8.078 (s, 2H), 5.672 (s, 2H), 4.173 (t, J = 7.6 Hz, 4H), 3.315 (m, 4H), 1.729 (m, 8H), 1.2−1.5 (m, 40H), 0.890 (m, 12H); mp 50−54 °C; $C_{56}H_{76}N_4O_4$ HRMS-ESI (*m*/*z*) [M + e] 868.5870 (calcd 868.5867). Anal. Calcd for $C_{56}H_{76}N_4O_4$: C, 77.38; H, 8.81; N, 6.45. Found: C, 77.18; H, 8.81; N, 6.37.

***N,N′*-Bis(*n*-octyl)-1,6-bis(*n*-octylamino)perylene-3,4:9,10-bis(dicarboximide):** ^{1}H NMR ($CDCl_3$, 500 MHz, see Figure S3, Supporting Information) δ 8.668 (d, J = 8.1 Hz, 2H), 8.594 (d, J = 8.1 Hz, 2H), 7.833 (s, 2H), 6.009 (s, 2H), 4.225 (t, J = 7.6 Hz, 2H), 4.178 (t, J = 7.6 Hz, 2H), 3.364 (t, J = 7.1 Hz, 4H), 1.78−1.64 (m, 8H), 1.25−1.5 (m, 40H), 0.898 (m, 12H); mp 50−55 °C; $C_{56}H_{76}N_4O_4$ HRMS-ESI (*m*/*z*) [M + e] 868.5870 (calcd 868.5867). Anal. Calcd for $C_{56}H_{76}N_4O_4$: C, 77.38; H, 8.81; N, 6.45. Found: C, 77.12; H, 8.66; N, 6.23.

***N,N′*-Bis(*n*-octyl)-1-(*n*-octylamino)perylene-3,4:9,10-bis(dicarboximide):** ^{1}H NMR ($CDCl_3$, 500 MHz) δ 8.667 (d, J = 8.1 Hz, 1H), 8.448 (d, J = 8.1 Hz, 1H), 8.350 (m, 1H), 8.216 (d, J = 7.9 Hz, 1H), 8.153 (m, 1H), 8.053 (m, 2H), 5.899 (s, 1H), 4.139 (m, 4H), 3.416 (m, 2H), 1.737, (m, 6H), 1.25−1.45 (m, 30H), 0.885 (m, 9H); mp 196−200 °C; $C_{48}H_{59}N_3O_4$ HRMS-FAB (*m*/*z*) 741.4506 (calcd 741.4506). Anal. Calcd for $C_{48}H_{59}N_3O_4$: C, 77.70; H, 8.01; N, 5.66. Found: C, 77.46; H, 7.97; N, 5.52.

Several arylene bis(dicarboximide)s having long alkyl chains are liquid crystalline (LC).[20,39,56,57] We explored the possibility of an LC phase for both the **1,6** and **1,7** isomers using differential scanning calorimetry. For both compounds there was no observable liquid crystalline transition between −40 and +350 °C.

Optical Spectroscopy. Steady-state absorption and emission spectra were acquired with a Shimadzu 1601 UV/vis spectrophotometer and PTI photon-counting spectrofluorimeter, respectively. A 10 mm quartz cuvette was used for both the absorption and fluorescence measurements. The fluorescence measurements were performed in a right angle configuration, and the optical density at λ_{max} was maintained at 0.05−0.1 to avoid reabsorption artifacts.

Electrochemistry and Spectroelectrochemistry. Electrochemical measurements were performed using an electrochemical workstation. All measurements were performed on isomerically pure compounds, confirmed by HPLC and NMR. The solvent used was methylene chloride (unstabilized HPLC grade passed through two columns of alumina) containing 0.1 M $TBAPF_6$. The electrochemical cell was fitted with a 1.0 mm diameter platinum disk working electrode, Ag/Ag_xO reference electrode, and platinum wire counter electrode, and was continuously purged with nitrogen during the measurements. The ferrocene/ferrocinium redox couple (Fc/Fc^+, 0.475 vs SCE) is used as an internal reference. Spectroelectrochemical measurements were also performed in methylene chloride with 0.1 M $TBAPF_6$ as described earlier.[21,58]

(56) Debije, M. G.; Chen, Z.; Piris, J.; Neder, R. B.; Watson, M. W.; Müllen, K.; Würthner, F. *J. Mater. Chem.* **2005**, *15*, 1270−1276.

(57) Struijk, C. W.; Sieval, A. B.; Dakhorst, J. E. J.; van Dijk, M.; Kimkes, P.; Koehorst, R. B. M.; Donker, H.; Schaafsma, T. J.; Picken, S. J.; van de Craats, A.; Warman, J. M.; Zuilhohf, H.; Sudholter, E. J. R. *J. Am. Chem. Soc.* **2000**, *122*, 11057−11066.

Electron Paramagnetic Resonance. EPR and ENDOR spectra were acquired with an EPR spectrometer, fitted with an ENDOR accessory, resonator, and RF power amplifier. Temperature was controlled by a liquid nitrogen flow system. Experimental parameters are provided in the captions of Figures 6 and 7. All samples, solvents, and oxidants were handled in a glovebox while purging with dry nitrogen. Methylene chloride (unstabilized HPLC grade passed through two columns of alumina) was stored over 3 Å molecular sieves in the drybox. The oxidant $NOSbF_6$ was used as received. This insoluble oxidant was added to a 1 mM solution of **(1,6)** or **(1,7)** in methylene chloride, and allowed to react for several minutes while agitating. The oxidation was halted by withdrawing the liquid, when ~25% of **(1,6**) or (**1,7**) had reacted (see UV−vis spectra, Figure S1, Supporting Information). A fraction of the oxidized solution was loaded into a 2.4 mm i.d. quartz tube which was then sealed in the glovebox with a 0.5−1.0 cm plug of vacuum grease, and wrapped tightly with Parafilm. UV−vis spectra acquired through the quartz tube match the spectra of the radical cations generated electrochemically. After 4 h at room temperature there was only a slight decrease in absorption of the radical cation as seen by UV−vis spectroscopy.

Electronic structure calculations were performed with Gaussian 98[59] installed on a Windows PC. Model compounds investigated by DFT had *N*-ethylamine groups attached to the PDI core, and methyl groups attached to the imide nitrogens. The structures of the neutral/radical cation were optimized with restricted/unrestricted DFT, incorporating the B3LYP functional and 6-31G* basis set. The isotropic hyperfine coupling constants of the radical cations were obtained after running a single point unrestricted DFT calculations with the B3LYP functional using the expanded double-ζ EPR-II basis set on the optimized radical cation structures.[60] The molecular volumes (and Onsager radii) were estimated by calculation at the AM1 level in Gaussian, employing the full molecules with the *n*-octyl substituents.

Acknowledgment. This work was supported by the Office of Naval Research under Grant No. N00014-05-1-0021. We thank Brooks Jones for assisting with DSC measurements, Jovan Giaimo for assistance with HPLC, Bryan Leavitt for assistance with fluorescence measurements, and Josh Vura-Weis for advice on the computations. M.J.T. acknowledges the donors of the American Chemical Society Petroleum Research Fund for partial support of this research. The Bruker E580 spectrometer was purchased with partial support from NSF Grant No. CHE-0131048.

Supporting Information Available: HPLC data, NMR, and UV−vis spectra as well as details of the DFT calculations. This material is available free of charge via the Internet at http://pubs.acs.org.

JO052394O

(58) van der Boom, T.; Hayes, R. T.; Zhao, Y.; Bushard, P. J.; Weiss, E. A.; Wasielewski, M. R. *J. Am. Chem. Soc.* **2002**, *124*, 9582−9590.

(59) Frisch, M. J.; Trucks, G. W.; Schlegel, H. B.; Scuseria, G. E.; Robb, M. A.; Cheeseman, J. R.; Zakrzewski, V. G.; Montgomery, J. A.; Stratmann, R. E.; Burant, J. C.; Dapprich, S.; Millam, J. M.; Daniels, A. D.; Kudin, K. N.; Strain, M. C.; Farkas, O.; Tomasi, J.; Barone, V.; Cossi, M.; Cammi, R.; Mennucci, B.; Pomelli, C.; Adamo, C.; Clifford, S.; Ochterski, J.; Petersson, G. A.; Ayala, P. Y.; Cui, Q.; Morokuma, K.; Malick, D. K.; Rabuck, A. D.; Raghavachari, K.; Foresman, J. B.; Cioslowski, J.; Ortiz, J. V.; Stefanov, B. B.; Liu, G.; Liashenko, A.; Piskorz, P.; Komaromi, I.; Gomperts, R.; Martin, R. L.; Fox, D. J.; Keith, T.; Al-Laham, M. A.; Peng, C. Y.; Nanayakkara, A.; Gonzalez, C.; Challacombe, M.; Gill, P. M. W.; Johnson, B. G.; Chen, W.; Wong, M. W.; Andres, J. L.; Head-Gordon, M.; Replogle, E. S.; Pople, J. A.; Gaussian, 5.2 ed.; Gaussian, Inc.: Pittsburgh, PA, 1998.

(60) Improta, R.; Barone, V. *Chem. Rev.* **2004**, *104*, 1231−1253.